Optimization of the National Biomass Allometric Equation Using Remote Sensing Data

Shweta Parajuli [1], Tarmo K. Remmel [1], Richard L. Bello [1]

[1] York University, Faculty of Environmental and Urban Change, Toronto, Ontario, Canada
shweta9@yorku.ca, remmelt@yorku.ca, bello@yorku.ca

Keywords: Allometric equation, Crown diameter, DBH, Individual tree detection, LiDAR

Abstract

Accurately estimating forest aboveground biomass is crucial for assessing its carbon sequestration and carbon emission capacity. However, the traditional approach to estimating biomass is time-consuming and labour-intensive. Therefore, remote sensing data are widely used to estimate forest biomass, with LiDAR being the most used. This study used available LiDAR and optical data to estimate aboveground biomass using an existing biomass allometric equation. The widely used allometric equations rely on DBH, height, and species information to estimate tree biomass. This study employed the DBH model and integrated LiDAR structural metrics and optical spectral bands to estimate aboveground biomass in a mixed-wood temperate forest. There was a moderate relationship between field-measured DBH and LiDAR estimated DBH, as indicated by a coefficient of determination of 0.52, the RMSE of 4.13 cm, and the MAE of 3.16. Additionally, combining LiDAR and optical data to estimate aboveground biomass yielded lower RMSE (115.4 Mg/ha) and MAE (96.8 Mg/ha) than using LiDAR alone, with 3.4% and 4.1% reductions, respectively. Overall, following the workflow presented in this study, the well-established allometric equation can be optimized for more scalable and larger extent forest biomass estimation.

1. Introduction

Forests are an essential part of the ecological environment. Accurately estimating their aboveground biomass (AGB) is essential for evaluating their capacity to store and release carbon and for understanding the carbon budget. (Liu et al., 2024). There are two basic approaches to biomass estimation: destructive and non-destructive. The destructive method involves cutting down the individual tree, whereas the non-destructive approach uses readily measurable field variables to estimate biomass via allometric relationships. The traditional destructive approach is most accurate, but it is also not feasible. Therefore, the allometric approach is the most widely accepted and adopted method for biomass estimation. However, a field-based allometric approach is labour-intensive and time-consuming. This is why Light Detection and Ranging (LiDAR) is used for biomass estimation: it can capture forest structural attributes and process data quickly. Today, we have easy access to airborne LiDAR data over large areas, making it essential to assess whether the tree metrics derived from it can act as predictor variables in the national allometric equation for larger-extent forest biomass estimation. The widely available allometric equations rely on DBH (diameter at breast height), height and species information of trees to estimate biomass (Lambert et al., 2005). However, obtaining DBH information from LiDAR is challenging in dense forests and requires high-point-density LiDAR data, which is typically obtained from terrestrial or handheld LiDAR devices (Mak et al., 2025). Only a few studies have developed an allometric model to estimate DBH from the metrics easily derivable from remote sensing data (Jucker et al., 2017), and only a limited number of studies have tested its effectiveness (Bhebhe et al., 2025). This study will focus on a bottom-up approach to biomass estimation and test DBH and height-derived biomass estimates from LiDAR data in mixed-wood forests in South Central. Ontario. The main objective of this study is to estimate forest biomass in a mixed-wood forest using the existing national AGB allometric equation, utilizing integrated LiDAR and optical data. Ultimately, this research answers the following questions: (1) How accurately can DBH be derived from LiDAR-based tree metrics in a heterogeneous mixed-wood forest? (2) What advantages are provided by integrating LiDAR and optical images for forest biomass estimates? (3) How effectively can the existing biomass allometric equations be utilized by remote sensing data?

2. Materials and methods

2.1 Study area

The study was conducted in South Ontario’s largest continuous forested swath, located at Canadian Forces Base (CFB) Borden, Figure 1. Hereafter will refer to it as Borden Forest. The site comprises relatively flat terrain in southern Ontario (44.3167°N, 79.9333°W). The area features a mixed temperate deciduous forest, which is regrowing on abandoned farmland from circa 1916. Borden Forest is in the Great Lakes–St. Lawrence Forest zone, with around 50% of its stems composed of red maple (*Acer rubrum*). Other dominant species in the forest include: large-tooth aspen (*Populus grandidentata*), trembling aspen (*Populus tremuloides*), Eastern white pine (*Pinus strobus*), red pine (*Pinus resinosa*), white and red ash (*Fraxinus americana* and *Fraxinus pennsylvanica*), and American beech (*Fagus grandifolia*) (Froelich et al., 2015). There is a 42 m tall eddy covariance (EC) flux tower situated close to the northern boundary of a roughly 5 km wide woodland that is encircled by agricultural areas and a military base (Froelich et al., 2015). To the north of the EC tower is a dual-aged pine plantation, as the abandoned farmland was planted approximately 90 years ago with red pine and Eastern white pine, and then thinned and replanted with the same species approximately 70 years ago. There is a narrow riparian zone traversing the forest from east to west, forming a valley containing Hemlock Creek (unofficial name), which is locally approximately 2 m lower in elevation than the surrounding terrain.

2.2 LiDAR and optical image data sources

High-density airborne LiDAR data (≥8 points/m²) and high-spatial resolution (16 cm) red, green, blue, and near-infrared (RBGN) imagery were obtained from the provincial geospatial repository (Ontario Geo Hub: https://geohub.lio.gov.on.ca/), collected during the spring of 2023.

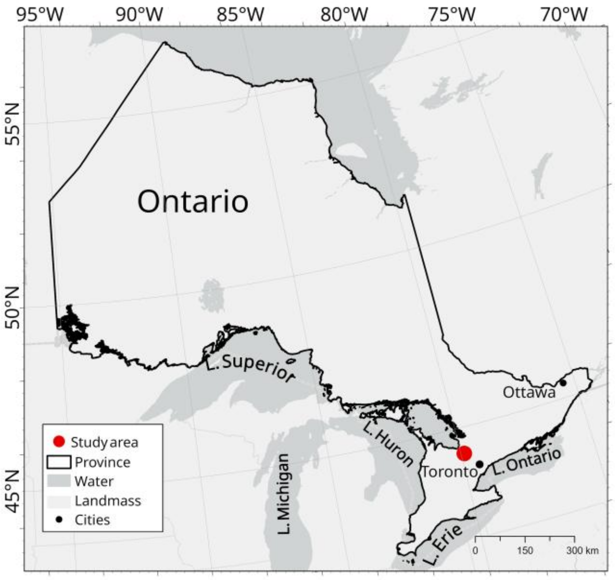

Figure 1. Map showing the location of the study area.

2.3 Field data collection

Field data were collected from the plots established over an area of 1.84 ha around the EC flux tower. The plot locations and transects were based on the historical wind rose and flux footprint data from the tower. Rectangular transects, as shown in Figure 2, are situated in the north, south, and west directions, with dimensions of 120 m × 40 m, 100 m × 40 m, and 240 m × 40 m, respectively, from the EC flux tower. Contiguous 20 × 20 m sample plots (single letters from A-W) with adjacent plots (double letters from AA-WW) made up each transect. There are 12, 10, and 24 sample plots in the North, South, and West transects, respectively, for a total of 46 plots.

All trees within the plots (DBH > 1cm) were inventoried, including species identification, status assessment (living or dead), and measurements of height and DBH. Altogether, data on over 3000 trees were collected in the field. The corner points for each plot were also collected using Real Time Kinematic (RTK) GPS location with horizontal positional accuracy of about 50 cm.

2.4 Forest type classification

Aerial images with RBGN bands were used to classify the study area into deciduous and coniferous forests. All bands present in the image, along with the normalized difference vegetation index, were used for classification. Supervised classification was used to classify the forest into two broad classes, and a small training sample was used for this study. Approximately 25-30 training samples per class were selected based on prior knowledge of the study area and the deciduous nature of the leafless trees. A random forest classifier was used for decision-making. To assess classification accuracy, samples were randomly split into training and validation sets, with half used for training and half for validation. Accuracy was assessed using a confusion matrix and overall accuracy. The classified image was downloaded in .TIFF file format which was used to determine the forest type of each crown. The classified raster was overlain on the LiDAR crown segments to determine which classification each crown fell under.

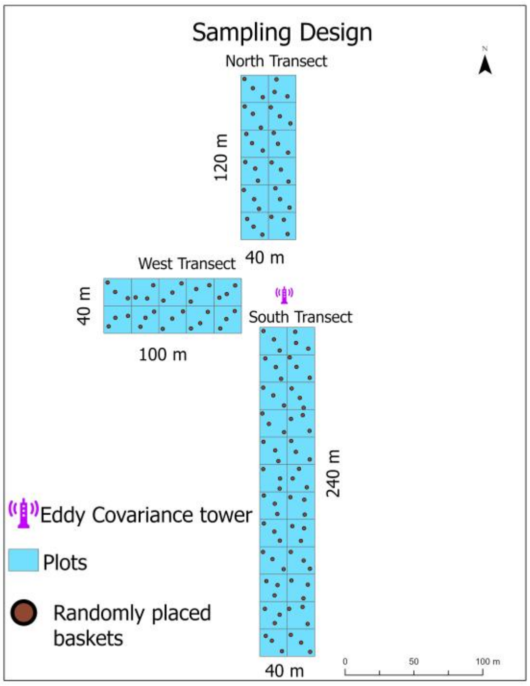

Figure 2. Schematic diagram representing the experimental design for the field data collection.

2.5 LiDAR data processing

An essential step in LiDAR data processing is classifying ground points from non-ground points. The downloaded LiDAR data was already classified into Classes 1, 2, 6, 7, and 18, corresponding to undefined, ground, building, noise, and high points, respectively. All the subsequent steps for the LiDAR data processing in this study were carried out using lidR package in R 4.4.3. (Roussel et al., 2020).

The next step after confirming the point cloud classification was to create the Digital Terrain Model (DTM). DTM was created using a Triangulated Irregular Network (TIN) approach. This approach for creating the elevation model generates irregular, non-overlapping triangles from known ground points to estimate values at unsampled locations. Since the interpolation from this approach is weak at the edges (i.e., it produces large, irregular triangles), a buffer area was used to generate the DTM and eliminate edge artifacts. The same algorithm, TIN, was used to create a Digital Surface Model (DSM). Finally, to get the exact height of the object (in this case, trees), we subtract the ground elevation from the surface model to create a Canopy Height Model (CHM). Hence, the CHM was developed by subtracting the derived DTM from the DSM. We constructed a 0.5 m resolution CHM, which was then smoothed using a kernel matrix to remove spurious local maxima caused by tree branches. Kernel smoothing is a linear averaging filter that smooths noise in the data by taking the weighted average of the neighbouring cells. The point clouds were also normalized to remove the influence of ground elevation. After CHM creation, tree segmentation was performed. Tree segmentation in LiDAR data processing mainly involves two steps: (1) Individual tree top detection, and (2) Crown segmentation. The individual treetops were detected in the normalized point cloud using the Local Maximum Filtering (LMF) algorithm. The algorithm uses the user-defined sliding window size as an input variable and detects the potential treetop. A variable window size was used for treetop detection in this study. The heights of the detected treetops were extracted to determine individual tree heights.

This study used Dalponte and Coomes, (2016), a crown segmentation algorithm, to segment the crown, using the detected tree top as a seed (Dalponte and Coomes, 2016). The algorithm segments a crown based on local maxima in the CHM.(Marcello et al., 2024). The user needs to define the maximum allowable crown diameter and the region-growing threshold. In this study, we used default values.

Once the crown was delineated, the selected crown segments were further used to extract the tree metrics. We extracted different percentile heights and crown metrics, including crown base height, from the segmented trees. We calculated the crown polygon area and the crown diameter, using the Equation (*1*), by assuming the crowns are circular to account for hidden coverage from overlapping (So et al., 2025).

$$CD = 2\sqrt{\frac{CA}{\pi}} \tag{1}$$

where CD is the diameter of the crown, and CA is the area of the crown polygon.

2.6 Diameter at breast height estimation

The DBH estimation model used in this research was developed by Jucker et al. (2017). The DBH model uses crown diameter and height as predictors of stem diameter. Jucker et al. (2017) chose a compound variable (i.e., height × crown diameter) and used binned data to model the allometric relationship between diameter and the compound variable. They fit a linear log-log model to binned data using least-squares regression. Since the binned data fails to capture the true variability of individual trees, the error term is included in the model (as shown in the Equation (2))

$$\ln(D) = \alpha + \beta \ln(H \times CD) + \varepsilon \tag{2}$$

According to Jucker et al. (2017), the allometric equation can be used to predict the stem diameter of individual trees when tree height and crown diameter are known.

$$D_{pred} = \exp[\alpha + \beta \ln(H \times CD) + \varepsilon] \tag{3}$$

(Jucker et al. (2017) assumed that ε follows a normal distribution (i.e., $N(0, \sigma^2)$) and expressed the mean of exp(ε) as $\exp(\sigma^2/2)$, and σ^2 represents the mean squared error of the regression. Hence, the diameter of the individual stem (*D*) can be predicted using the Equation (4).

$$D_{pred} = \exp[\alpha + \beta \ln(H \times CD)] \times \exp\left[\frac{\sigma^2}{2}\right] \tag{4}$$

which was calculated to be:

$$D_{pred} = 0.557 \times 0.809\,(H \times CD) \times \exp\left[\frac{0.0562}{2}\right] \tag{5}$$

Based on this, the study used the allometric equation to predict the tree's DBH from LiDAR-derived individual tree height and crown diameter.

2.7 Forest aboveground biomass estimation

This study used the biomass allometric equation developed by Lambert et al. (2005) to estimate the total aboveground biomass. Lambert et al. (2005) has developed an allometric model for total aboveground biomass across 33 tree species in Canada. All species in our study area are included in his model. Total aboveground biomass in his model is estimated by summing the component biomass of the tree (as shown in Equation (6)), which is calculated by relating DBH and height to their respective biomass.

$$T_{AGB} = T_{wood} + T_{bark} + T_{foliage} + T_{branches} \tag{6}$$

where T_{AGB} is the total aboveground biomass, T_{wood}, T_{bark}, $T_{foliage}$, and $T_{branches}$ are the biomass of compartments: wood, bark, foliage and branches, respectively.

To estimate aboveground biomass from field data, we used a species-specific allometric equation. The forest inventory data (i.e., species information), DBH, and height, were used for the calculations. When the absence of leaves, bark or branching patterns prevented identification to species, we used a general allometric equation to estimate foliar biomass.

For remote sensing data, we were able to differentiate between deciduous and coniferous forests, but we did not have enough data to separate them into species. Lambert et al. (2005) has also developed a forest-type-specific as well as a general allometric equation. These equations were developed to accommodate tree species for which biomass allometric equations have not been developed. We used the forest-type-specific allometric equation they developed to estimate aboveground biomass from LiDAR-derived tree height and predicted DBH.

2.8 Model validation and error analysis

The tree metrics and biomass estimates derived from LiDAR and optical data were evaluated using model-fit statistics, including the coefficient of determination (R^2), root mean square error (RMSE), and mean absolute error (MAE). The models were evaluated based on higher R^2 values, and lower RMSE and MAE.

$$R^2 = 1 - \frac{SS_{res}}{SS_{tot}} \tag{7}$$

where SS_{res} is the residual sum of squares and SS_{tot} is the total sum of squares. The sum of residuals tells us how far the actual values are from the predicted values, whereas the total sum of squares tells us how far the actual values are from the mean of the dependent variable.

$$\text{RMSE} = \sqrt{\frac{1}{n}\sum_{i=1}^{n}(y_i - \hat{y}_i)^2} \tag{8}$$

here y_i is the observed value for observation *i*, $\hat{y}_i$ is the predicted value for observation *i*, and *n* is the total number of observations.

$$\text{MAE} = \frac{1}{n}\sum_{i=1}^{n}|y_i - \hat{y}_i| \tag{9}$$

here y_i is the observed value for observation *i*, $\hat{y}_i$ is the predicted value for observation *i*, and *n* is the total number of observations.

3. Results and Discussion

3.1 Estimation of DBH from LiDAR metrics

The height and crown diameter were the predictor variables for DBH estimation. Since the field inventory included all trees with DBH > 1 cm, first, LiDAR-derived mean tree heights for each plot were compared with field-measured mean tree heights using different DBH thresholds. Trees having a DBH ≥ 15 cm showed a higher coefficient of determination (R^2= 0.7), lower RMSE (2.67 cm) and MAE (2.0 m), shown in Table *1*, when compared to the mean tree height from LiDAR. Hence, subsequent estimates derived from remote sensing data were compared with field data for trees with DBH ≥ 15 cm. As anticipated, the mean tree height comparison across different DBH thresholds indicates that LiDAR detected larger trees in the field and failed to detect understorey (DBH <15 cm).
There was a moderate relationship between field-measured DBH and LiDAR estimated DBH (as shown in Figure *3*). We found R^2 = 0.52, RMSE = 4.13 cm, and MAE = 3.16 cm. The North transect, which is a plantation forest and had mostly coniferous trees, showed better agreement with the mean DBH of the field, with lower RMSE (3.1 cm) and MAE (2.7 cm) than the West and South transect, naturally regenerated forest (RMSE of 4.5 cm and MAE of 3.3 cm). A higher error was observed around the creek, where the tree stems were mostly inclined.

Table 1. Comparison of LiDAR-predicted mean tree height with field-measured mean tree height after applying different DBH thresholds to filter trees in the field.

DBH threshold (m)	R^2	RMSE (m)	MAE (m)
10	0.66	3.36	2.7
12	0.65	2.98	2.2
15	**0.67**	**2.67**	**2.0**
20	0.62	2.92	2.3
25	0.50	3.75	3.0
30	0.35	4.71	3.7

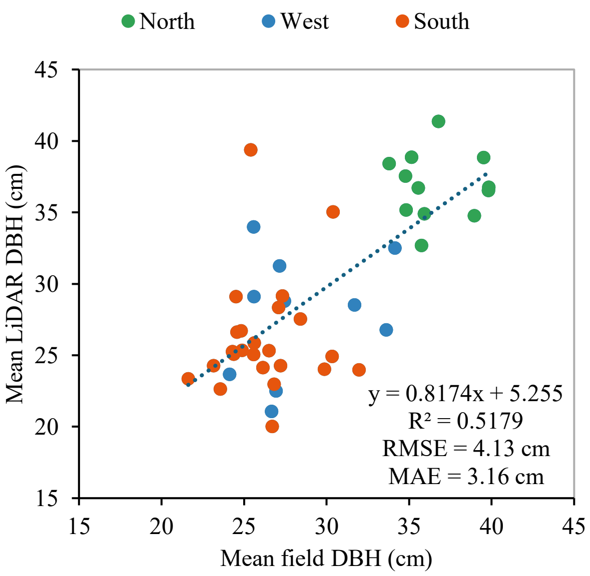

Figure 3. Comparison of mean DBH estimated from LiDAR data against field-measured DBH across 46 plots.

3.2 Classified forest type from aerial image

The Figure 4 shows the classification result map for the study area. To classify the forest type as coniferous or deciduous, approximately 25-30 training sample points per forest type were used. However, half of the samples were used for training, and the other half for testing the classification model. As shown in the results, the North transect is dominated by conifers. Similarly, the West transect shows the dominance of deciduous trees, whereas the South transect depicts a mixed deciduous-coniferous forest. As shown in the figure, the Hemlock Creek in the south transect is dominated by coniferous forest. In contrast, the areas where plots L to O are located are dominated by deciduous forest in the south transect. This finding is similar to the field observation.
The statistical result of the findings is shown in Table 2. According to this, 1.03 ha of the forest (56.4% of the study area) is occupied by deciduous trees, whereas 0.79 ha (43.4%,) is occupied by coniferous trees.
A confusion matrix was generated to evaluate classification accuracy. Half of the sample points were used for testing, and an overall accuracy of 0.98 was achieved, indicating strong predictive performance on the test data. The F1 score was also calculated to assess the classification's accuracy. The F1 score for deciduous and coniferous forest was 0.95 and 0.98, respectively. The classification results closely matched the observed forest type in the study area.

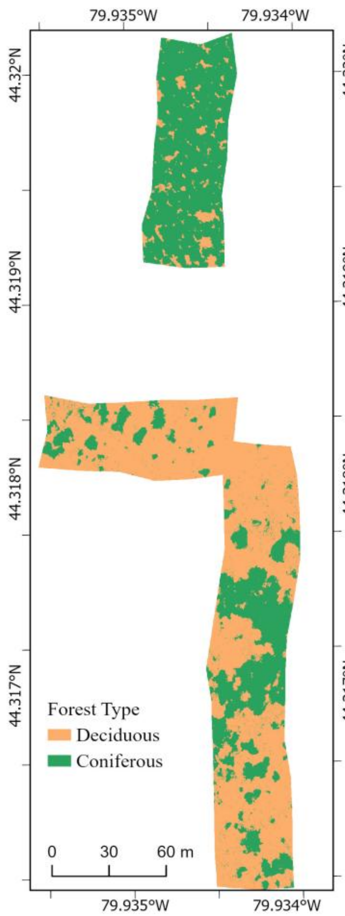

Figure 4. Map representing the classification of the study area into deciduous and coniferous forest type using optical data.

This contribution has been peer-reviewed.
https://doi.org/10.5194/isprs-archives-XLIX-B3-2026-1037-2026

Table 2. The area of each forest type, in hectares, resulted from the supervised classification of the aerial imagery.

Forest type	Total area (ha)	% of total study area
Deciduous	1.028	56.4
Coniferous	0.792	43.4

3.3 Estimation of aboveground biomass from LiDAR data

LiDAR-estimated DBH and height were used to estimate total AGB using a general allometric equation from Lambert, which was compared with field-measured total aboveground biomass using a species-specific allometric equation (Figure 5). When forest type information was not included in the aboveground biomass estimation from LiDAR, the relationship between LiDAR aboveground biomass and field aboveground biomass was moderate, as indicated by the R^2 = 0.48, RMSE = 119.4 Mg/ha and MAE = 101.0 Mg/ha. Similarly, when compared the mean AGB from field with LiDAR estimated mean AGB, we found very low RMSE (3.9 Mg/ha) and MAE (2.89 Mg/ha). This result indicates that LiDAR metrics alone can moderately explain variation in the field-estimated aboveground biomass of tree species in our study area. Overall, LiDAR underestimated total aboveground biomass, particularly in plots with higher aboveground biomass per hectare. The observed R^2 in this study is similar to the R^2 observed in the study by Osei Darko et al. (2025), where they observed an R^2 = 0.42 in a Canadian temperate forest using a machine-learning modelling approach. This also indicates that a simple workflow replicating the field-based biomass estimation approach can produce a similar estimate of aboveground biomass.

3.4 Estimation of aboveground biomass from combined LiDAR and optical data

We did not have species information for the trees; however, we had forest-type information from the optical data. The forest type information was overlain on the LiDAR data to determine the individual tree's forest type information. We compared the aboveground biomass estimated using a forest-type-specific allometric equation from Lambert, derived from a combination of LiDAR and optical data. Figure 6 shows a linear regression of aboveground biomass from remote-sensing data against field measurements. The result showed an R^2 = 0.45, slightly lower than that obtained when only LiDAR metrics were used for aboveground biomass estimation. However, we observed lower RMSE (115.4 Mg/ha) and MAE (96.8 Mg/ha) with integrated remote sensing data than with LiDAR alone. This represented a 3.4% reduction in RMSE and a 4.1% reduction in MAE. The reduction observed appears minimal in a small study, but it may become significant when biomass estimates are extrapolated to larger spatial extents. Additionally, when compared the mean AGB from the field with remote sensing data we found very low RMSE (3.8 Mg/ha) and MAE (2.85 Mg/ha). This indicates that incorporating forest-type information into LiDAR metrics improves total aboveground biomass estimates, with the potential for significant improvement across larger areas. Additionally, RMSE and MAE were compared between the plantation forest and the naturally regenerated forest. The RMSE and MAE were 110.1 Mg/ha and 87.6 Mg/ha, respectively, for naturally regenerated forests, which were lower than those for plantation forests (RMSE = 129.0 Mg/ha and MAE = 122.9 Mg/ha). This finding contradicted our initial assumption, as structural attributes, such as tree height and DBH, showed less bias in the plantation forest than in the naturally regenerated forest. We compared the relative root mean square error (rRMSE) between plantation and naturally regenerated forests and found that rRMSE was higher for natural forests (53%) than for plantation forests (37%). This result indicates that the plantation forest had higher absolute error due to greater biomass magnitude but lower relative error, which indicates better proportional accuracy. Overall, the results show that aboveground biomass can be estimated from integrated remote sensing data using established biomass allometric equations and a DBH model, without developing a site-specific model.

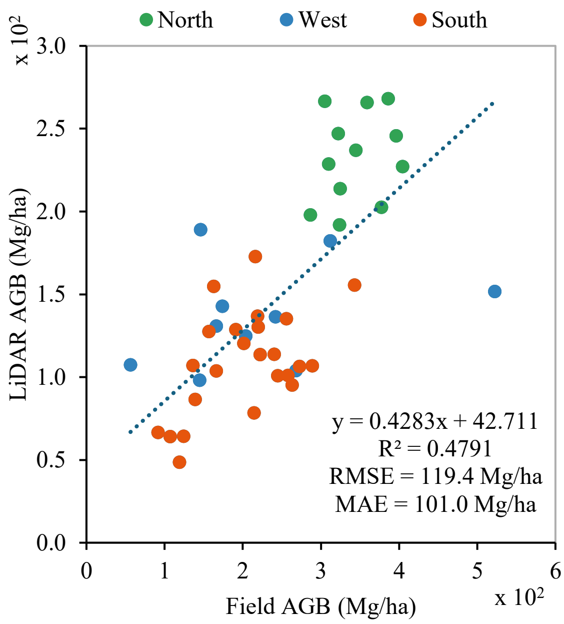

Figure 5. Comparison of the mean aboveground biomass estimated by using LiDAR height and DBH against the mean field estimated aboveground biomass.

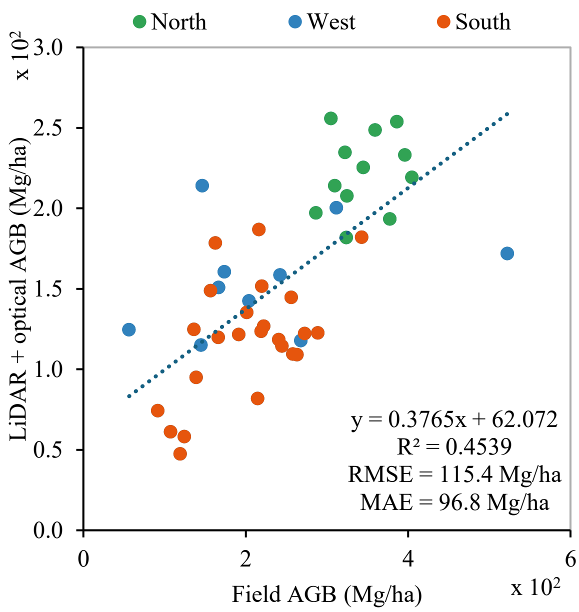

Figure 6. Comparison of the mean aboveground biomass estimated by using LiDAR structural attribute and optical forest type information against the mean field estimated aboveground biomass.

4. Conclusions

This study assessed the feasibility of estimating total aboveground biomass from remote sensing data using the existing national biomass allometric equation, without establishing a local biomass model based on field data. The results showed that the existing national allometric equation can be applied using remote-sensing-derived variables. The DBH model performed well in mixed-wood temperate forests, and the results showed that plantation conifer forests had lower RMSE (3.1 cm) and MAE (2.7 cm) than naturally regenerated deciduous-dominated forests (RMSE = 4.5 cm and MAE = 3.3 cm). Overall, when we replicate field inventory using remote sensing data, such as individual tree identification, extracting their structural attributes, and determining their forest type, we are essentially doing what we have been doing for a long time in the field. This enables optimization of the well-established allometric equation, and we found that, following the workflow presented in this study, we achieved lower RMSE and comparable coefficient of determination to those reported in studies that modelled biomass from remote sensing variables. This approach is more effective for conifer plantations, with a lower rRMSE (37%), than naturally regenerated mixed forests dominated by deciduous trees, which showed a higher rRMSE of 53%, even though the absolute error was higher for the plantation than the natural forest. This may be due to the distinct structural differences between conifers and the fact that our plantation forest comprised only two conifer species, whereas we had more than five deciduous species, each with its own structural attributes and biomass accumulation capacity. Furthermore, if tree species can be distinguished using LiDAR or optical data, this may improve biomass estimation. Similarly, most crown segmentation algorithms perform better for coniferous tree species. Developing forest-type-specific crown segmentation algorithms could improve DBH estimates from the DBH model, as DBH strongly correlates with biomass. Overall, this research demonstrates that the established biomass allometric equation can be used to effectively estimate forest biomass. With the increasing availability of LiDAR and optical data, this method becomes more scalable and closely aligned with field estimates.

5. Acknowledgements

The authors thanks Canadian Space Agency [24AO3YOR35] and the NSERC Discovery Grant [RGPIN-2021-03645] for funding this project. Special thanks to Environment and Climate Change Canada and Canadian Forces Base Borden for providing access to the research site.

6. References

Bhebhe, Z.M., Liu, X., Zhang, Z., Paudyal, D.R., 2025. Estimation of Tree Diameter at Breast Height (DBH) and Biomass from Allometric Models Using LiDAR Data: A Case of the Lake Broadwater Forest in Southeast Queensland, Australia. *Remote Sensing 17*, 2523. https://doi.org/10.3390/rs17142523

Dalponte, M., Coomes, D.A., 2016. Tree-centric mapping of forest carbon density from airborne laser scanning and hyperspectral data. *Methods Ecol Evol 7*, 1236–1245. https://doi.org/10.1111/2041-210X.12575

Froelich, N., Croft, H., Chen, J.M., Gonsamo, A., Staebler, R.M., 2015. Trends of carbon fluxes and climate over a mixed temperate–boreal transition forest in southern Ontario, Canada. *Agricultural and Forest Meteorology* 211–212, 72–84. https://doi.org/10.1016/j.agrformet.2015.05.009

Jucker, T., Caspersen, J., Chave, J., Antin, C., Barbier, N., Bongers, F., Dalponte, M., van Ewijk, K.Y., Forrester, D.I., Haeni, M., Higgins, S.I., Holdaway, R.J., Iida, Y., Lorimer, C., Marshall, P.L., Momo, S., Moncrieff, G.R., Ploton, P., Poorter, L., Rahman, K.A., Schlund, M., Sonké, B., Sterck, F.J., Trugman, A.T., Usoltsev, V.A., Vanderwel, M.C., Waldner, P., Wedeux, B.M.M., Wirth, C., Wöll, H., Woods, M., Xiang, W., Zimmermann, N.E., Coomes, D.A., 2017. Allometric equations for integrating remote sensing imagery into forest monitoring programmes. *Glob Chang Biol 23*, 177–190. https://doi.org/10.1111/gcb.13388

Lambert, M.-C., Ung, C.-H., Raulier, F., 2005. Canadian national tree aboveground biomass equations. *Can. J. For. Res. 35*, 1996–2018. https://doi.org/10.1139/x05-112

Liu, X., Dong, L., Li, S., Li, Z., Wang, Y., Mao, Z., Deng, L., 2024. Improving AGB estimations by integrating tree height and crown radius from multisource remote sensing. *PLoS ONE 19*, e0311642. https://doi.org/10.1371/journal.pone.0311642

Mak, N.P.L., Siu, T.Y., Law, Y.K., Zhang, H., Sui, S., Yip, F.T., Ng, Y.S., Ye, Y., Cheung, T.C., Wa, K.C., Chan, L.H., So, K.Y., Hau, B.C.H., Lee, C.K.F., Wu, J., 2025. Mapping Individual Tree- and Plot-Level Biomass Using Handheld Mobile Laser Scanning in Complex Subtropical Secondary and Old-Growth Forests. *Remote Sensing 17*, 1354. https://doi.org/10.3390/rs17081354

Marcello, J., Spínola, M., Albors, L., Marqués, F., Rodríguez-Esparragón, D., Eugenio, F., 2024. Performance of Individual Tree Segmentation Algorithms in Forest Ecosystems Using UAV LiDAR Data. *Drones 8*, 772. https://doi.org/10.3390/drones8120772

Osei Darko, P., Metari, S., Arroyo-Mora, J.P., Fagan, M.E., Kalacska, M., 2025. Application of Machine Learning for Aboveground Biomass Modeling in Tropical and Temperate Forests from Airborne Hyperspectral Imagery. *Forests 16*, 477. https://doi.org/10.3390/f16030477

Roussel, J.-R., Auty, D., Coops, N.C., Tompalski, P., Goodbody, T.R.H., Meador, A.S., Bourdon, J.-F., de Boissieu, F., Achim, A., 2020. lidR: An R package for analysis of Airborne Laser Scanning (ALS) data. *Remote Sensing of Environment 251*, 112061. https://doi.org/10.1016/j.rse.2020.112061

So, K., Chau, J., Rudd, S., Robinson, D.T., Chen, J., Cyr, D., Gonsamo, A., 2025. Direct Estimation of Forest Aboveground Biomass from UAV LiDAR and RGB Observations in Forest Stands with Various Tree Densities. *Remote Sensing 17*, 2091. https://doi.org/10.3390/rs17122091